Chemical Engineering Science 320 (2026) 122444

Contents lists available at ScienceDirect

Chemical Engineering Science

journal homepage: www.elsevier.com/locate/ces

Development of a two-dimensional Raman spectroscopy measuring technique for the visualization of mass transfer during droplet formation

Franziska Bertram [a,*], Jörg Hofmann [b], Jan Gottschalk [b], Felix Weißenberg [c], Thorsten Brands [c], Carlo Holly [b,d], Andreas Jupke [a,e,*]

[a] RWTH Aachen University, Fluid Process Engineering (AVT.FVT), 52074 Aachen, Germany
[b] RWTH Aachen University, Chair for Technology of Optical Systems (TOS), 52074 Aachen, Germany
[c] RWTH Aachen University, Institute of Technical Thermodynamics (LTT), 52062 Aachen, Germany
[d] Fraunhofer Institute for Laser Technology (ILT), 52074 Aachen, Germany
[e] Forschungszentrum Jülich GmbH, Institute for Bio- and Geosciences (IBG-2), 52428 Jülich, Germany

ARTICLE INFO

Keywords:
Raman measuring setup
Droplet formation
Mass transfer
Local concentration measurements
Optical design

ABSTRACT

A novel two-dimensional Raman spectroscopy measurement setup is developed to visualize mass transfer during droplet formation and applied to the water/acetonitrile/toluene system. This setup enables direct observation of local solute contents. Experiments were conducted using 2 mm and 4 mm droplets with an initial acetonitrile content of 10 wt%. The results are qualitatively consistent with findings reported in the literature for similar systems. Initial calibration measurements using single-phase systems demonstrated linear correlations between measured intensities and solute contents in both phases, though a baseline shift in the organic phase was attributed to the presence of toluene. Applying these correlations to droplet formation experiments resulted in an overestimation of local acetonitrile contents. Future work will focus on further refining the quantification capabilities of the measurement setup.

1. Introduction

Liquid-liquid extraction is a separation process based on differing distribution of dissolved substances between two immiscible or only partially miscible liquid phases. It is widely employed for isolating target components from complex mixtures, with applications including chemical, petrochemical, biochemical, hydrometallurgical and nuclear separations processes (Gebauer et al., 2016).

Measuring mass transfer in individual droplets is crucial for gaining deeper insights into key aspects of liquid–liquid extraction processes. Despite considerable progress in measurement techniques, accurately quantifying and understanding mass transfer at the micro-scale within individual droplets remains challenging. Optical measurement methods provide a promising, non-invasive and fast way to capture two-dimensional concentration profiles (Ambrosini and Ferraro, 2018). While various measuring techniques are currently available, they all indirectly assess the concentration of the transferring component.

Laser-induced fluorescence (LIF) has been applied repeatedly to measure the mass transfer in single-droplet in the water/acetone/toluene system (Heine and Bart, 2019; 2020; Heine et al., 2021; Wang et al., 2021); as well as selected other systems (Heine and Bart, 2020; Heine et al., 2021; Wang et al., 2021). For this measuring technique a fluorescent dye, e.g. rhodamine 6G when acetone is used as solute, is added to the system. Fluorescence is induced using a two-dimensional laser sheet and measured orthogonally to the laser sheet plane. The concentration of the transfer component can thus be calculated from the measured fluorescence intensity. It is assumed that the dye behaves exactly like the solute and does not affect the extraction process. This technique has also been applied to the measurement of mass transfer of a rising bubble (Weiner, 2019). Using a rotating polygon, even three-dimensional concentration profiles have been obtained (Rüttinger et al., 2018).

Kögl (Kögl) investigated the mass transfer in the water-hydrogen chloride/methyl isobutyl ketone-tributyl phosphate system with iron ions (Fe^{3+}) as solute using X-ray computed tomography. For this measuring technique the measuring cell is irradiated with X-rays. The emitted photons interact with the sample. This causes scattering or absorption of the photons, therefore attenuating the transmitted energy. The degree of attenuation depends on the density and atomic number of the present chemicals, whereas a high atomic number leads to higher attenuation. The transmitted energy is recorded by a detector. By

* Corresponding authors.
E-mail addresses: Franziska.Bertram@avt.rwth-aachen.de (F. Bertram), Andreas.Jupke@avt.rwth-aachen.de (A. Jupke).

https://doi.org/10.1016/j.ces.2025.122444
Received 3 July 2025; Received in revised form 29 July 2025; Accepted 15 August 2025
Available online 16 August 2025

Nomenclature

Symbols

d	[mm] Diameter
δz	[mm] Distance to image focal plane

Sub- and Superscripts

i	Inner
o	Outer

Abbreviations

ACN	Acetonitrile
CWL	Central wavelength
FHMW	Full width at half maximum
LIF	Laser-induced fluorescence
SI	Supplementary Information
Tol	Toluene

superimposing several images recorded from different angles, the local concentration distribution may be inferred by tomographic reconstruction (Kögl; Seeram, 2023). This measuring technique is also suitable for three-dimensional measurements by using multiple rows of detectors to capture several slices simultaneously; or by translating the measuring volume being scanned relatively to the source-detector pair, a method commonly used in medicine (Nikolaou et al., 2019).

Another technique used for measuring single droplets is Schlieren photography. Here, the sample is illuminated by a light source. The local refractive index depends on the local solute concentration and thus on the concentration of the transfer component. Due to the different refractive indices in the beam path, the rays are deflected to varying degrees, as captured by a camera. There are different measuring techniques with varying experimental setups (Settles and Hargather, 2017). Two of the more commonly used setups, Knife-edge Schlieren photography and Rainbow or Color Schlieren photography, have been used to investigate mass transfer in the water/acetone/toluene system (Heine et al., 2021; Mao et al., 2023; Schulz et al., 2018). Agble and Mendes-Tatsis (Agble and Mendes-Tatsis, 2000) used Schlieren photography to investigate the effect of surfactants on the interfacial mass transfer of single droplets for different organic phases. A three-dimensional resolution can be achieved using tomographic reconstructions (Srivastava, 2013). However, this technique only provides information on the concentration profile outside the droplet.

A different approach for the measurement of two-dimensional concentration profiles is Raman spectroscopy. For this measuring technique, the sample is irradiated with a monochromic laser source leading to Raman scattering. The scattered photons have either a higher frequency, known as anti-Stokes Raman scattering, a lower frequency, known as Stokes Raman scattering, or the same frequency, known as Rayleigh scattering, than the laser photons (Mallick, 2023). The spectral distribution of the Raman signal is substance-specific and can be used for identification and for direct concentration measurements (Kudelski). For analytical applications, Stokes Raman scattering is generally preferred due to its higher intensity compared to anti-Stokes Raman scattering. (Mallick, 2023; Kudelski).

Raman spectroscopy has many applications in the fields of chemistry, physics, material sciences, mineralogy, and archelogy, biology, biochemistry, pharmacy as well as biomedicine (Schmitt and Popp, 2006). Heine and Bart used confocal Raman spectroscopy to measure mass transfer during droplet formation in the water/acetonitrile/toluene system yielding the temporal concentration profile for a small measuring volume within the droplet (Heine and Bart, 2017).

To obtain a two-dimensional spatially resolved concentration profile using Raman spectroscopy, the local Raman signal scattered by the sample needs to be measured, resulting in a three-dimensional measuring space. In literature, there are four main methods for spatially resolved spectral imaging which are shown schematically in Fig. 1: Whiskbroom, Pushbroom, Staring and Snapshot (Li et al., 2013). When applying the Whiskbroom method, or point-scanning method, each local point is scanned individually. For two-dimensional imaging, the sample is shifted relative to the detector, or vice versa. This method is used for confocal Raman microscopy (Da Gomes Costa et al). In the Pushbroom method, or line scanning method, the spectral information is recorded simultaneously for all points along one spatial coordinate. Both methods are too time-consuming in scanning a 2-dimensional plane to capture the dynamic effects of mass transport in single droplets. In contrast, with the Staring method, or band sequential method, the entire two-dimensional space is measured at the same time. This method uses filters to measure only light of one wavelength at a time. The snapshot, or single-shot, method is designed to capture both spatial and spectral information on an area detector in a single exposure by remapping and dispersing image zones onto the detector. This approach is the fastest way to capture the entire three-dimensional data cube. However, spatial and spectral resolution is limited due to sensor size.

In this paper, we present a measuring setup using two-dimensional Raman spectroscopy designed to measure the mass transfer in single droplets. As spectral imaging approach, the Staring method has been selected. This approach has been used extensively in the analysis of gas jets (Braeuer et al., 2009; Gragston et al., 2019; Jiang et al., 2017; 2018; Wu, 2024). With this non-invasive measuring setup, it is possible to directly measure the local concentration distribution of the transition component without the addition of a fluorescent dye. Since the measuring setup uses narrow bandpass filters, it is possible to investigate different chemical systems. The prerequisite for a signal separation of different substances is the existence of a peak in the Raman spectra that can clearly be assigned to the solute and is spectrally separated from other peaks. The water/acetonitrile/toluene system was identified as a suitable candidate. Due to the high interfacial tension, the used system is prone to exhibit Marangoni convection (Marangoni). The primary goal of our research is to develop and validate this new method, demonstrating its feasibility and effectiveness in a proof of principle.

The signals obtained with Raman spectroscopy are often several magnitudes less intense than those obtained with LIF (Mazilu et al., 2010). Therefore, a key component of the measuring setup is the lens system focusing the scattered Raman signal onto the camera. The design thereof and the influence of the droplet radius and its position relative to the image focal plane on the image quality will be discussed first. Then, droplet formation experiments with varying droplet diameters will be presented, followed by a characterization of the setup's overall quantification capabilities. Finally, a first quantification approach is applied to the droplet formation experiments.

2. Material and methods

2.1. Chemicals and analytics

For all experiments a liquid–liquid system consisting of toluene as dispersed phase, acetonitrile as solute, and water as continuous phase was used. The system behaves similar to the standard test system for liquid extraction studies water/acetone/toluene (Misek et al., 1985); with the mass transfer being slightly faster for acetonitrile (Heine and Bart, 2020). The Raman spectrum for acetonitrile (top) and toluene (bottom) when excited with a wavelength of 532 nm are shown in Fig. 2. The spectrum of acetonitrile exhibits a peak at a wavelength of 604.4 nm (2252 cm^{-1}) which is due to C≡N stretching (Neelakantan, 1964); whereas neither toluene nor water (Carey and Korenowski, 1998) show any peaks in that wavelength range. This peak can thus be used for unambiguous identification of acetonitrile in the system at hand.

Toluene (Tol) with a purity of ≥ 99.8 % (VWR) and acetonitrile (ACN) with a purity of ≥ 99.98 % (Carl Roth) were used. High purities

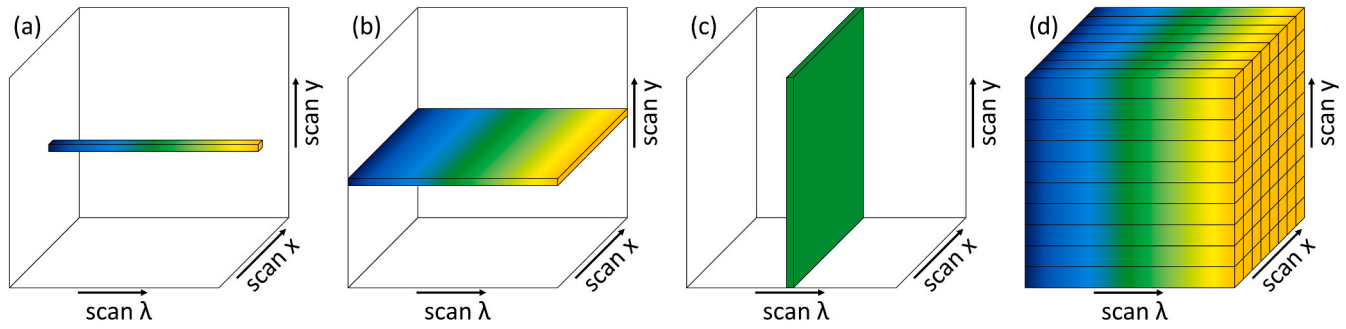

Fig. 1. Schematic representation of typical spectral imaging approaches. Adapted from (Li et al., 2013). (a) Whiskbroom. (b) Pushbroom. (c) Staring. (d) Snapshot.

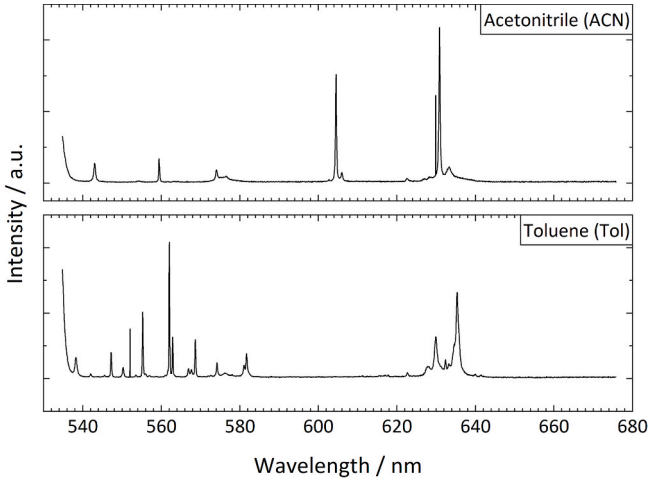

Fig. 2. Raman spectra of acetonitrile (top) and toluene (bottom). Measured intensities for an excitation wavelength of 532 nm.

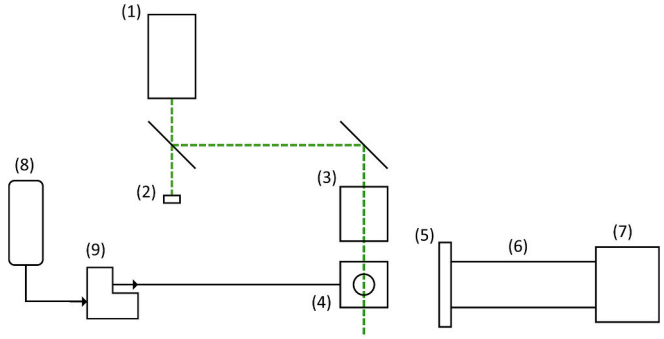

Fig. 3. Experimental setup. (1) laser, (2) power sensor, (3) optics, (4) measurement cell, (5) filter wheel with bandpass filters, (6) optics, (7) camera, (8) storage tank, (9) precision syringe pump.

were chosen to reduce the impact of impurities on mass transfer. Deionized water (conductivity 0.8 µS/cm), further purified via distillation (Puridest 4 G, LAUDA Dr. r. Wobser GmbH&Co.KG) was used for all experiments.

Due to the applied Staring method, the full Raman spectra cannot be analyzed within the presented Raman measuring setup. Therefore, the full Raman spectra were measured using a Virsa™ Raman-Analyser (Renishaw plc) with a laser power of 22.5 mW, an excitation wavelength of 532 nm, a groove density of 2400 l/mm, and a camera exposure time of 2 s. The transmission degrees of the bandpass filters were measured using a UV–Vis Spectrometer (UV-2401PC, Shimadzu Deutschland GmbH).

2.2. Description of the Raman spectroscopy measuring setup and method

The principle of the two-dimensional Raman measuring setup is shown schematically in Fig. 3. An additional picture of the experimental setup can be found in the SI. For excitation, a laser (1) with a maximum laser power of 52.5 W (GLR-532–50-SF, IPG Laser GmbH) and a wavelength of 532 nm is being used. The emitted laser power was measured using a power sensor (2) (S121C, Thorlabs Inc.), with the laser intensity showing a standard deviation of approximately 1 % over a 4-minute period. The beam is shaped by several optics (3) into a laser sheet with a nominal height of 10 mm and a nominal width of 0.1 mm. The laser sheet passes through the measuring cell (4) (LBC-LC-98-I-30, BIOZOL GmbH). The measuring cell has internal dimensions of 30 × 30 × 30 mm and is made of IR quartz. The scattered Raman signal passes through a custom-made bandpass filter (5) (Chroma Technology Corp) with the central wavelength (CWL) of 604.4 nm and a FHMW of 1.7 nm and is focused on a camera (7) (camera resolution 2048 × 2048 pixel, maximum frame rate at full resolution 100 fps, pco.edge 4.2 AIR CLHS, PCO AG) using a custom-made lens system (6). The whole setup is designed to have a visual field of 10 × 10 mm, leading to a spatial resolution of the measuring plane of 4.9 × 4.9 µm/pixel. All experiments were carried out at room temperature (23.1 ± 0.3 °C). To eliminate background signal contributions from the camera sensor, a dark-frame correction was applied. For this, 1000 frames were recorded without laser excitation. The average of these frames was used as a dark-frame and subtracted from each raw Raman image. This approach ensures that the resulting Raman images represent only the true optical signal from the measuring plane.

To minimize mass transfer of toluene and water during droplet formation, both phases were mutually saturated prior to the addition of acetonitrile. For this purpose, toluene and water were dispersed and allowed to equilibrate overnight, followed by a settling period of one hour. After phase separation, acetonitrile was added gravimetrically to the respective phases.

For droplet formation experiments, the measurement cell was filled with the saturated continuous phase. The droplets consisting of disperse phase and solute were induced via a glass capillary (d_i = 1.3 mm, d_o = 3.3 mm, Aachener Quarzglas-Technologie Heinrich GmbH & Co. KG) using a syringe pump (9) (PSD/6, Hamilton Bonaduz AG). A sketch of the measuring volume is included in the SI. Measurements were performed using the maximum laser power of 52.5 W and a camera exposure time of 100 ms. A solute content of 10 wt% acetonitrile and droplet diameters of 2 mm and 4 mm were chosen. The droplets were injected with a formation rate of 0.6 $\mu L s^{-1}$.

For calibration, the measurement cell was filled with either saturated water or saturated toluene, containing varying acetonitrile concentrations. The acetonitrile contents in both phases investigated ranged from 0 wt% to 50 wt%. Measurements were performed using the maximum laser power of 52.5 W and camera exposure times of 10 ms, 50 ms and 100 ms. Each measurement was carried out over 100 frames to reduce measurement noise.

2.3. Optical design

The laser sheet illuminating the measuring cell was set to a nominal height of 10 mm and a nominal width of 0.1 mm. The laser source emits a beam with a diameter of 0.82 mm, requiring vertical expansion by a factor of 12.2 and a horizontal narrowing of the laser beam by a factor of 0.122. The former was achieved using an anamorphic telescope with two cylindrical lenses. As for the latter, the beam is focused in the direction of observation of the camera using a single cylindrical lens.

The design of the lens system for focusing the scattered Raman signal onto the camera was performed using Ansys Zemax OpticStudio. This included accounting for refractive index changes at various optical interfaces, such as the spherical aberrations introduced by the curved droplet surface, the cuvette, and the bandpass filter. These aberrations were compensated for by the lens design. A sketch of the optical setup for droplet observation, along with a simulation of individual rays, is shown in Fig. 4.

The primary design goal of the lens system was to minimize spherical aberration caused by the curved interphase of the droplet, ensuring a sharp image of individual droplets. To evaluate imaging quality, a pattern of letters was simulated in the measuring plane inside the droplet using Ansys Zemax OpticStudio. The emitted light rays from the measuring plane are then captured by the imaging lens system and focused on the camera chip.

The simulated performance of the lens system for droplet diameters of 1 mm, 2 mm, and 3 mm is shown in Fig. 5. The top images demonstrate the effect of different droplet diameters on imaging quality. Although the optical system was optimized for a droplet diameter of 2 mm, the letter pattern remains clearly recognizable for 1 mm and 3 mm droplets, indicating that droplets of varying sizes can be effectively investigated.

The bottom images demonstrate the influence of the droplet's position relative to the image focal plane for a 2 mm droplet. Simulations show that when the droplet forms outside the focus, the letters appear distorted. This distortion is evident, for example, in the varying line widths of the letter "N". These findings highlight the importance of forming the droplet within the laser sheet's focus to ensure accurate measurements.

3. Results and discussion

3.1. Droplet formation measurements

Due to the shaping of the incoming laser, the laser intensity assumes a Gaussian shape along the height and width of the laser sheet. Furthermore, the laser sheet expands slightly along its path. The resulting Raman images exhibit stripes along the laser propagation direction, which originate from the laser sheet itself. An exemplary distribution of intensity values for 50 wt% acetonitrile in water is shown in Fig. 6. The corresponding distribution of relative standard deviations can be found in the SI. For further analysis, the variation in laser intensity along the direction of laser propagation is assumed to be negligible.

Raman spectral image sequences of two droplet formation experiments as recorded by the 2D-Raman spectroscopy measuring setup are shown in Fig. 7 and Fig. 8. Both droplets were induced with an initial acetonitrile content of 10 wt% and a formation rate of 0.6 μLs^{-1}. The droplet in Fig. 7 was set to reach a final diameter of 2 mm, whereas the droplet in Fig. 8 reached a final diameter of 4 mm. Both sequences were recorded with a camera exposure time of 100 ms. Since the smaller droplet is located in the lower region of the measuring plane, where the laser intensity is reduced, the color scale for both figures were chosen differently. Due to the minor local rise in acetonitrile content in the aqueous phase and a signal offset present in the organic phase, the local increase of Raman intensity in the aqueous phase resulting from mass transfer is not discernible in either figure. An exemplary Raman spectral image of the 4 mm toluene droplet at 53.8 s with an adapted color scale to highlight the increase in Raman signal is provided in the SI.

At the beginning of the droplet formation, the droplets are depleted in acetonitrile. This is evident at 1.2 s for the 2 mm droplet (Fig. 7) where the droplet exhibits areas with very low Raman intensity. This initial depletion occurs due to mass transfer taking place immediately after the phases come into contact, even before droplet formation starts. As fresh disperse phase is added during the injection process, the measured Raman intensities within the droplet increase and become more uniform, as seen at 5 s. The injection process stops after 7.6 s. Beyond this point, the droplet starts to decrease in size as the acetonitrile content decreases with ongoing mass transfer from the organic to the aqueous phase. Shortly after the injection process stops, the first vortices appear in the lower region of the droplet, noticeable at 9.8 s. The vortices grow and change position within the droplet (13.6 s), until they become virtually stable in the lower region of the droplet. In addition to the vortices within the droplet, Marangoni eruptions were observed, accompanied by intense lateral oscillations. At 37.6 s the highest intensities can be found in the middle of the droplet and at the interface at the top of the droplet, implying a central inflow of acetonitrile due to a post-carriage effect. These observations align with the ones made by Heine and Bart (Heine and Bart, 2019) for the water/acetone/toluene system. After 244 s, the measured intensities are still of the same magnitude. This is assumed to result from the large inner diameter of the capillary used, leading to a significant post-carriage effect and therefore to a prolonged mass transfer.

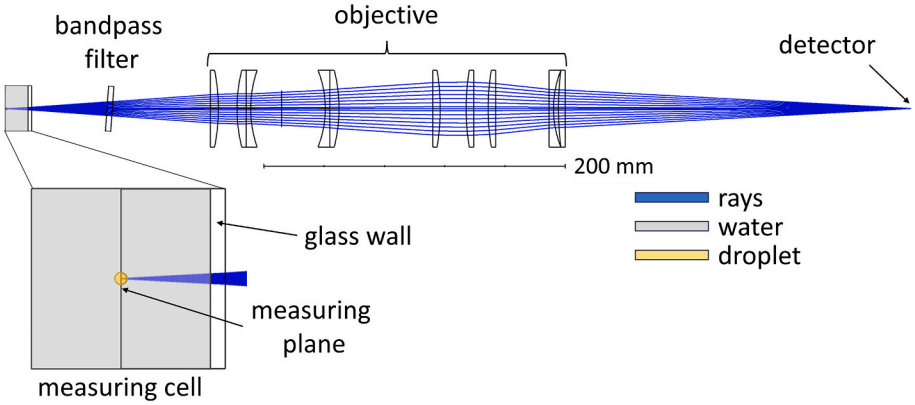

Fig. 4. Sketch of the measuring cell and the optical system used for droplet observation. The droplet phase is shown in orange, the aqueous phase in grey, and the simulated individual rays of scattered Raman signal in blue. (For interpretation of the references to color in this figure legend, the reader is referred to the web version of this article.)

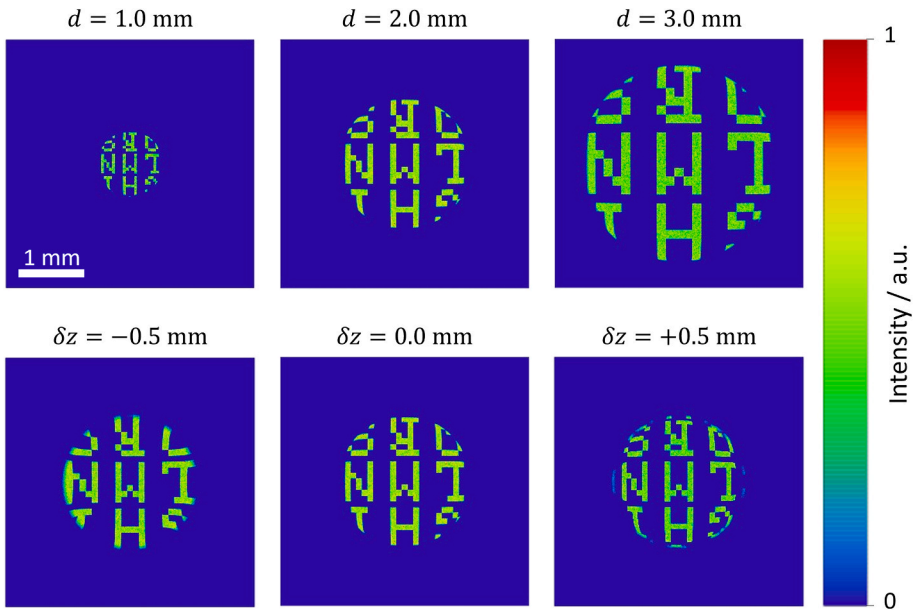

Fig. 5. Influence of the droplet radius d (top row) and the horizontal distance of the droplet to the image focal plane δz (bottom row) on the image quality.

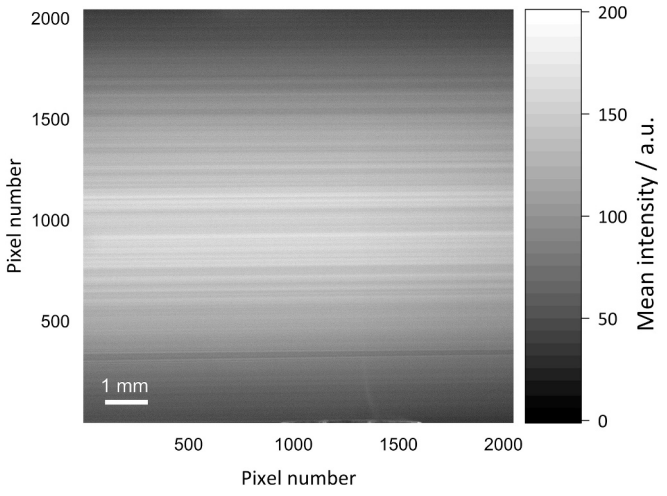

Fig. 6. Exemplary mean Raman intensities of 50 wt% acetonitrile in water averaged over 100 frames. Measured with a camera exposure time of 100 ms and a bandpass filter with a CWL of 604.4 nm.

The droplet with a final diameter of 4 mm as shown in Fig. 8 exhibits a similar behavior to the 2 mm droplet. The measured Raman intensity within the droplet is initially low but increases with ongoing injection of new disperse phase. Notably, the first vortices appear well before the end of the injection process, visible at 11.2 s. These vortices grow and stabilize during injection, likely due to the incoming organic phase inducing internal flow within the droplet. The Raman spectral image captured at 53.8 s shows the droplet shortly before injection stops at 54.6 s. Directly above the capillary, a triangular area of high Raman intensity is observed as highlighted by the white rectangle. By 56.6 s, shortly after the injection ceases, this area has disappeared while the rest of the Raman intensity profiles remain largely unchanged. Once the injection has stopped, the vortices shift throughout the droplet forming various patterns, as seen at 73.4 s and 92 s. Eventually, the vortices stabilize again in the lower part of the droplet. At 143.2 s and 244 s, a post-carriage effect is observed, although its magnitude appears smaller than that noted for the 2 mm droplet.

3.2. Characterization of the measuring setup

For the characterization of the measuring setup, a first quantification approach using continuous phases was chosen. To this end, the measuring volume was filled with either saturated water or saturated toluene with differing acetonitrile contents, and the spatially dissolved Raman intensities were measured with varying camera exposure times. The obtained pixel intensity values for the upper 2000-pixel rows of the Raman images were averaged to obtain a single value. This number was chosen to exclude the glass capillary in the bottom region of the measuring setup. To minimize the influence of measurement noise, each measurement was carried out and averaged over 100 individual frames. All measurement series display an offset of at least 100 a.u., which increases with increasing camera exposure time. Preliminary tests indicate that most of this offset originates from the camera itself, with a smaller contribution resulting from the laser sheet, the latter varying with camera exposure time. The corresponding measurement series are provided in the SI. To account for the signal contribution from the camera, a dark-frame correction has been applied. The resulting mean Raman intensities are shown in Fig. 9. The left-hand figure contains the values obtained for the aqueous system, whereas the right-hand figure for the organic system. The standard deviations for the mean intensity values are all below 1 %, indicating reproducibility of the measurements. Furthermore, the standard deviation was calculated for each pixel to estimate local measurement noise. To obtain a representative value for the overall noise in the measuring plane, the standard deviations of the upper 2000-pixel rows were averaged. The resulting mean standard deviation is shown as error bars in Fig. 9. A spatially resolved example of the local standard deviation distribution is provided in the SI.

Both the aqueous and the organic phase exhibit a linear relationship between the acetonitrile content and the measured Raman intensity. In both cases, the measurement noise as represented by the error bars increases with longer camera exposure times and higher acetonitrile content. Linear regression lines were fitted to all measurement series, as shown in Fig. 9. The slopes of the regression lines for each camera exposure time are of the same order of magnitude for both the aqueous and organic phases. However, the two phases show different offsets. To understand where the difference in the offset stems from, the Raman spectra for varying acetonitrile contents in pure toluene have been measured. An excerpt of the spectra between 602 nm and 612 nm are shown in Fig. 10. All spectra display a baseline offset that increases with

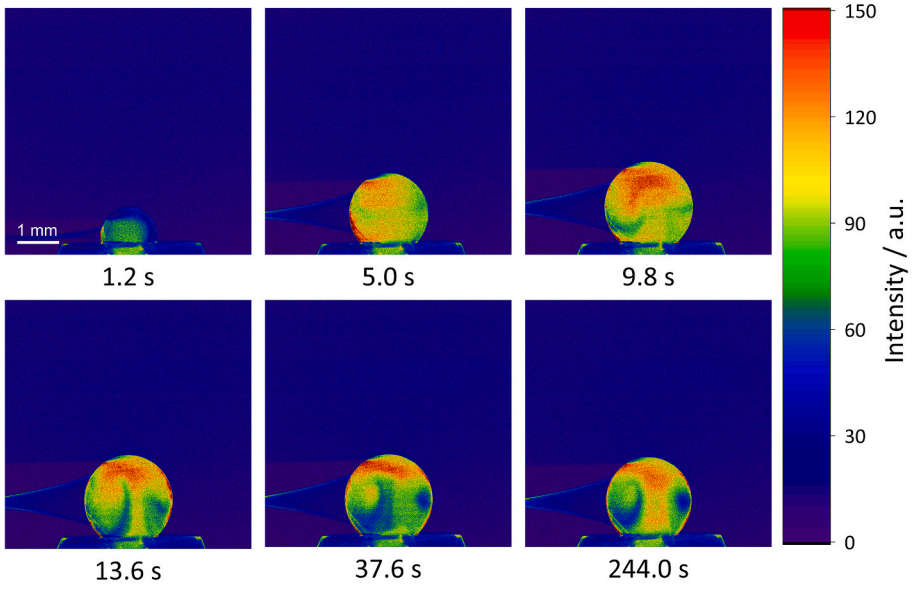

Fig. 7. Raman images of a 2 mm toluene droplet at different time steps during droplet formation with an initial acetonitrile content of 10 wt% and a formation rate of 0.6 μLs^{-1}. Images were obtained using a bandpass filter with a CWL of 604.4 nm.

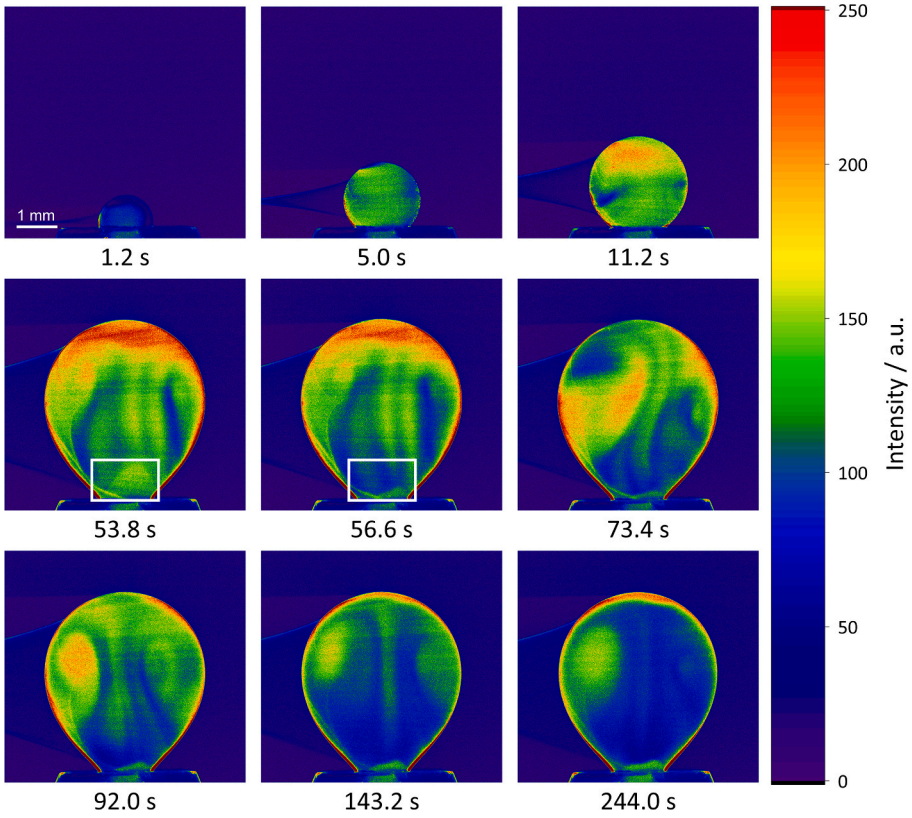

Fig. 8. Raman images of a 4 mm toluene droplet at different time steps during droplet formation with an initial acetonitrile content of 10 wt% and a formation rate of 0.6 μLs^{-1}. Images were obtained using a bandpass filter with a CWL of 604.4 nm.

decreasing acetonitrile content and can therefore be attributed to the presence of toluene. This baseline shift must be accounted for in any potential quantification, for example by using separate calibrations for the aqueous and organic phase.

3.3. Quantification of the droplet formation experiments

To quantify the individual Raman images obtained during droplet formation experiments, a row-wise calibration of the Raman images using a linear model was selected to account for the Gaussian distribution of laser intensity along the height of the measuring plane. The Raman intensities obtained at a camera exposure time of 100 ms were

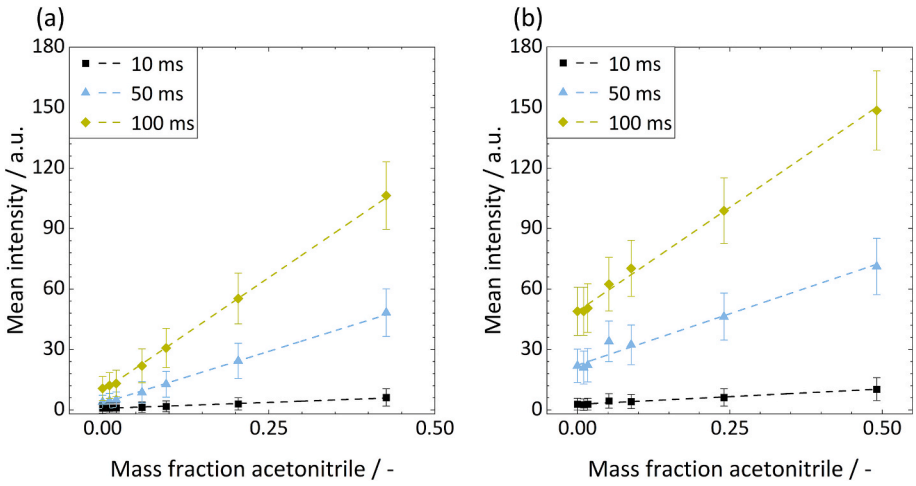

Fig. 9. Mean Raman intensities for different acetonitrile content in water (a) and acetonitrile in toluene (b) for different camera exposure times measured with CWL of 604.4 nm.

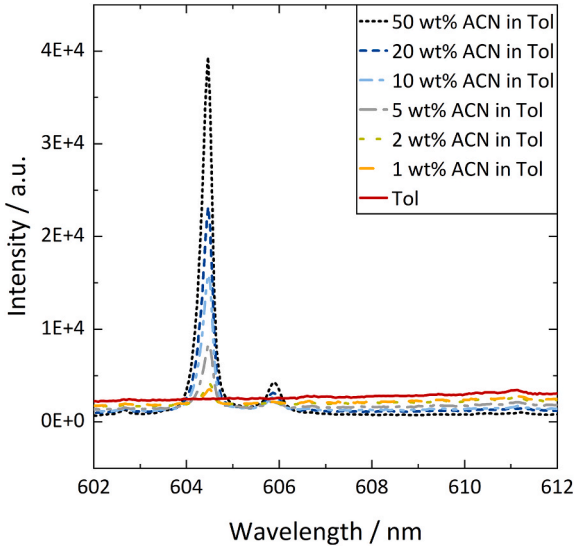

Fig. 10. Detail excerpt of the Raman spectra of different acetonitrile contents in toluene ranging from 602 nm to 612 nm.

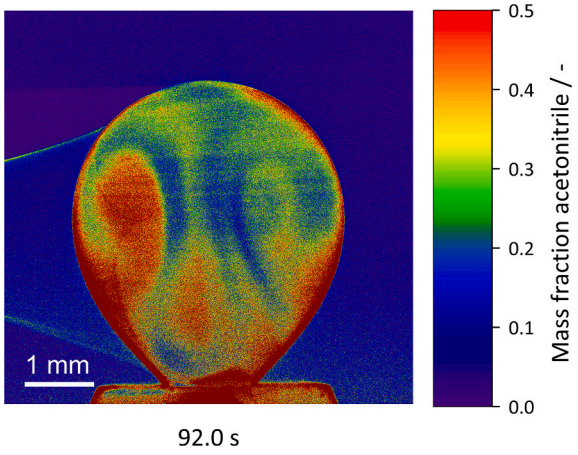

Fig. 11. Local content profile of a 4 mm toluene droplet with 10 wt% acetonitrile with a formation rate of 0.6 μLs^{-1} at 92 s. The content of the aqueous and the organic phase were calculated separately using a line-wise calibration approach.

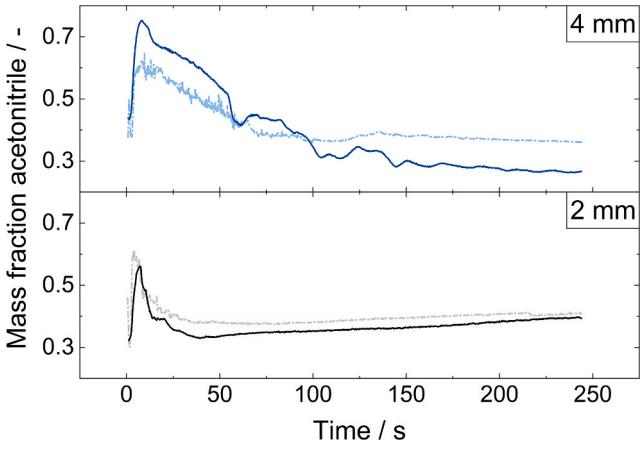

Fig. 12. Temporal evolution of mean droplet content, averaged over the 2D measurement plane. 4 mm toluene droplet shown in dark blue and 2 mm toluene droplet shown in black. Repetition experiments are shown in light blue and grey. All droplets were injected with a formation rate of 0.6 μLs^{-1} and an initial ACN-content of 10 wt%. (For interpretation of the references to color in this figure legend, the reader is referred to the web version of this article.)

averaged over 100 frames for each row, and a linear regression was performed for each individual row. The resulting parameters linking the measured Raman intensity to the acetonitrile content are provided in the SI. To separate the organic phase from the aqueous phase the MATLAB k-means tool was used. The numbers of pixels attributed to the organic phase were calculated and plotted over time. Outliers were identified based on a strongly deviating number of pixels and excluded manually. The number of pixels over time, including the outliers, are shown in the SI. The line-wise calibration was then applied to each phase separately. The resulting local acetonitrile distribution for the 4 mm droplet at 92 s is shown in Fig. 11.

The mean acetonitrile content of the droplet, averaged over the measuring plane, was calculated for each frame and plotted over time. The results only include the contents within the measuring plane and do not account for the three-dimensional structure of the droplet. The result can be seen in Fig. 12. The black line corresponds to the 2 mm droplet shown in Fig. 7, while the dark blue line represents the 4 mm droplet depicted in Fig. 8. Overall, the calculated acetonitrile contents are overestimated, with values reaching up to 75 wt%. This overestimation is attributed to the spherical phase boundary, where the laser is refracted towards the droplet's center. This refraction increases local

laser intensities within the camera's focal plane, leading to higher Raman intensities. This effect could not be replicated during calibration in a continuous organic phase. Further quantification approaches will have to take this effect into account, e.g. by using a biphasic system.

Nevertheless, the progression of the content over time qualitatively confirms several observations made from the Raman images. Both profiles start with relatively low acetonitrile content, attributed to mass transfer taking place before droplet formation. In the case of the 2 mm droplet, the acetonitrile content increases, reaching a peak around 7.2 s, just before the injection process stops. After this point, the acetonitrile content decreases rapidly, reaching a local minimum at approximately 40 s, before starting to increase again. The increase is likely caused by the post-carriage effect, which introduces additional acetonitrile into the droplet. For the 4 mm droplet, the acetonitrile content begins at a higher level than that of the 2 mm droplet, suggesting less mass transfer occurred prior to droplet formation. Both acetonitrile content profiles reach their maximum value around the same time, before starting to decrease again. As for the 2 mm droplet, the acetonitrile content decrease is faster than for the 4 mm droplet, assumably due to the lower surface-to-volume ratio of the 4 mm droplet. The acetonitrile content profile of the 4 mm droplet exhibits fluctuations, with the acetonitrile content increasing over a short period of time before decreasing again. This is attributed to the asymmetrical distribution of acetonitrile within the three-dimensional droplet. Regions with higher acetonitrile contents can move into and out of the measuring plane, causing variations in the measured two-dimensional acetonitrile content. Apart from those fluctuations, the acetonitrile content continues to decline throughout the entire measurement period, showing no significant post-carriage effect.

Both droplet formation experiments were repeated, with the results shown in grey for the 2 mm droplet and in light blue for the 4 mm droplet. While the starting acetonitrile contents and the maximum acetonitrile contents differ between the droplets, the overall trends align with those observed in the initial experiments, indicating qualitatively good reproducibility of the results.

4. Conclusion and outlook

In this study, we introduced a Raman spectroscopy measurement setup for the spatially resolved analysis of solute content during droplet formation. The applied Raman spectroscopy measuring technique enables direct assessment of solute content without requiring auxiliary substances such as fluorescent dyes. For proof-of-principle, the system water/acetonitrile/toluene was selected. The excitation laser sheet was configured with a nominal height of 10 mm and a nominal width of 0.1 mm. The lens system, designed to image the area illuminated by the excitation laser onto the camera, was optimized to minimize spherical aberration caused by the droplet's curved interphase.

The setup can be adapted to study mass transfer in other liquid-liquid extraction systems. To this end, the transfer component should exhibit a distinct, narrow Raman peak without spectral overlap with either phase, and the bandpass filter should be selected to match that peak while accommodating potential peak shifts caused by variations in the experimental conditions. Furthermore, incorporating a second camera system into the setup would allow for simultaneous measurement of multiple solute contents.

Droplet formation experiments revealed the formation of inner vortices, Marangoni convection, and the presence of a post-carriage effect. These findings align with observations reported in the literature for the water/acetone/toluene system. The measuring setup was evaluated for its quantification potential, establishing a linear relationship between intensity values and solute content in both the aqueous and organic phase. However, a baseline shift attributed to toluene was observed in the organic phase. This baseline shift may be addressed indirectly by calibrating the aqueous and organic phases separately or directly by measuring the Raman intensity using a second bandpass filter with a central wavelength near the acetonitrile peak.

Applying the calibration to droplet formation experiments revealed acetonitrile contents up to 7.5 times higher than the initial acetonitrile content in the organic phase. This discrepancy was attributed to changes in local laser intensities caused by light refraction at the curved droplet interphase. Further quantification will require direct calibration of the organic phase using droplets of varying diameters, which will be addressed in future work. Alternatively, a ratiometric measurement would also be conceivable, in which the disadvantages of the inhomogeneous local laser intensity are overcome by measuring a reference peak of known concentration.

CRediT authorship contribution statement

Franziska Bertram: Writing – review & editing, Writing – original draft, Visualization, Methodology, Investigation, Formal analysis, Data curation, Conceptualization. **Jörg Hofmann:** Writing – review & editing, Writing – original draft, Methodology, Investigation, Data curation. **Jan Gottschalk:** Methodology, Data curation. **Felix Weißenberg:** Writing – review & editing, Data curation. **Thorsten Brands:** Writing – review & editing, Supervision. **Carlo Holly:** Writing – review & editing, Supervision. **Andreas Jupke:** Writing – review & editing, Supervision, Funding acquisition, Conceptualization.

Declaration of competing interest

The authors declare that they have no known competing financial interests or personal relationships that could have appeared to influence the work reported in this paper.

Acknowledgment

Funded by the Deutsche Forschungsgemeinschaft (DFG, German Research Foundation) under Germany's Excellence Strategy – Cluster of Excellence 2186 "The Fuel Science Center" – ID: 390919832

Appendix A. Supplementary data

Supplementary data to this article can be found online at https://doi.org/10.1016/j.ces.2025.122444.

Data availability

Data will be made available on request.

References

Gebauer, F., Hlawitschka, M.W., Bart, H.-J., 2016. CFD aided investigation of single droplet coalescence. Chin. J. Chem. Eng. 24 (2), 249–252. https://doi.org/10.1016/j.cjche.2015.07.024.

Ambrosini, D., Ferraro, P., 2018. Here, there and everywhere: the art and science of optics at work. Opt. Lasers Eng. 104, 1–8. https://doi.org/10.1016/j.optlaseng.2018.01.009.

Heine, J.S., Bart, H.-J., 2020. Local analysis of Marangoni effects during and after droplet formation. Can. J. Chem. Eng. 98 (5), 1164–1171. https://doi.org/10.1002/cjce.23685.

Heine, J.S., Bart, H.-J., 2019. Visualization of mass transfer during droplet formation. Chem. Eng. Technol. 42 (7), 1388–1394. https://doi.org/10.1002/ceat.201800706.

Heine, J.S., Schulz, J.M., Junne, H., Böhm, L., Kraume, M., Bart, H.-J., 2021. Real-time visualization of internal and external concentration fields in multiphase systems via laser-induced fluorescence and rainbow Schlieren deflectometry during and after droplet production. Chem. Ing. Tech. 93 (1–2), 180–190. https://doi.org/10.1002/cite.202000135.

Wang, Z., Chen, J., Feng, X., Mao, Z.-S., Yang, C., 2021. Visual dynamical measurement of the solute-induced Marangoni effect of a growing drop with a PLIF method. Chem. Eng. Sci. 233, 116401. https://doi.org/10.1016/j.ces.2020.116401.

Weiner, A., et al., 2019. Experimental and numerical investigation of reactive species transport around a small rising bubble. Chem. Eng. Sci.: X 1, 100007. https://doi.org/10.1016/j.cesx.2019.100007.

Rüttinger, S., Spille, C., Hoffmann, M., Schlüter, M., 2018. Laser-induced fluorescence in multiphase systems. ChemBioEng Rev. 5 (4), 253–269. https://doi.org/10.1002/cben.201800005.

Kögl, T., "Tomographische Untersuchungen in der flüssig-flüssig Extraktion," Doctoral dissertation, Friedrich-Alexander-Universität Erlangen-Nürnberg (FAU).
Seeram, E., 2023. X-Ray Imaging Systems for Biomedical Engineering Technology. Springer International Publishing, Cham.
Nikolaou, K., Bamberg, F., Laghi, A., Rubin, G.D., 2019. Multislice CT. Springer International Publishing, Cham.
Settles, G.S., Hargather, M.J., 2017. A review of recent developments in schlieren and shadowgraph techniques. Meas. Sci. Technol. 28 (4), 42001. https://doi.org/10.1088/1361-6501/aa5748.
Mao, Q., Yang, Q.-J., Liu, Y., Cao, W., 2023. Experimental and numerical study of droplet formation with Marangoni instability. Chem. Eng. Sci. 268, 118369. https://doi.org/10.1016/j.ces.2022.118369.
Schulz, J.M., Junne, H., Böhm, L., Kraume, M., 2018. Development of an Experimental Setup Applying Rainbow Schlieren Deflectometry for Visualization and Quantification of Heat and Mass Transfer in Multiphase Systems. Proceedings of the 5th International Conference on Experimental Fluid Mechanics, Munich.
Agble, D., Mendes-Tatsis, M.A., 2000. The effect of surfactants on interfacial mass transfer in binary liquid–liquid systems. Int. J. Heat Mass Transf. 43 (6), 1025–1034. https://doi.org/10.1016/S0017-9310(99)00184-2.
Srivastava, A., 2013. Development and application of color schlieren technique for investigation of three-dimensional concentration field. J. Cryst. Growth 383, 131–139. https://doi.org/10.1016/j.jcrysgro.2013.09.001.
Mallick, P.K., 2023. Fundamentals of Molecular Spectroscopy. Springer Nature Singapore, Singapore.
Kudelski, A., "Analytical applications of Raman spectroscopy," Talanta, early access. doi: 10.1016/j.talanta.2008.02.042.
Schmitt, M., Popp, J., 2006. Raman spectroscopy at the beginning of the twenty-first century. Journal of Raman Spectroscopy: JRS 37 (1–3), 20–28. https://doi.org/10.1002/jrs.1486.
Heine, J.S., Bart, H.-J., 2017. Mass transfer during droplet formation – a measuring technique study. Chem. Ing. Tech. 89 (12), 1635–1641. https://doi.org/10.1002/cite.201700045.
Li, Q., He, X., Wang, Y., Liu, H., Xu, D., Guo, F., 2013. Review of spectral imaging technology in biomedical engineering: achievements and challenges. J. Biomed. Opt. 18 (10), 100901. https://doi.org/10.1117/1.JBO.18.10.100901.
Da Gomes Costa, S., Richter, A., Schmidt, U., Breuninger, S., Hollricher, O., "Confocal Raman microscopy in life sciences," Morphologie : bulletin de l'Association des anatomistes, early access. doi: 10.1016/j.morpho.2018.12.003.
Braeuer, A., Engel, S.R., Hankel, R.F., Leipertz, A., 2009. Gas mixing analysis by simultaneous Raman imaging and particle image velocimetry. Opt. Lett. 34 (20), 3122–3124. https://doi.org/10.1364/OL.34.003122.
Gragston, M., et al., 2019. Simultaneous Species Concentration and Flow Velocity Imaging Using 2D Raman Scattering at Elevated Pressure, in AIAA Scitech 2019 Forum, San Diego, California, doi: 10.2514/6.2019-1325.
Jiang, N., et al., 2017. High-speed 2D Raman imaging at elevated pressures. Opt. Lett. 42 (18), 3678–3681. https://doi.org/10.1364/OL.42.003678.
Jiang, N., et al., 2018. High-Speed, Two-dimensional, Multi-species Raman Imaging for Combustion and Flow Diagnostics, in 2018 AIAA Aerospace Sciences Meeting, Kissimmee, Florida, doi: 10.2514/6.2018-2040.
Wu, B., et al., 2024. High-speed 1-D and 2-D Raman scattering measurement for quantitative characterization of transient hydrogen jets. Proc. Combust. Inst. 40 (1–4), 105417. https://doi.org/10.1016/j.proci.2024.105417.
Marangoni, C., "Marangoni, Carl. "Ueber die Ausbreitung der Tropfen einer Flüssigkeit auf der Oberfläche einer anderen.," Annalen der Physik, vol. 219, no. 7, pp. 337–354.
Mazilu, M., de Luca, A.C., Riches, A., Herrington, S., Dholakia, K., 2010. Modulated Raman spectroscopy technique for real-time fluorescence rejection, in Imaging, Manipulation, and Analysis of Biomolecules, Cells, and Tissues VIII, San Francisco, California, D. L. Farkas, D. V. Nicolau, and R. C. Leif, Eds., 2010, 75680M, doi: 10.1117/12.841675.
Misek, T., Berger, R., Schröter, J., 1985. Standard test systems for liquid extraction studies. EFCE Publication Series 46.
Neelakantan, P., 1964. Raman spectrum of acetonitrile. Proc. Indian Acad. Sci. 60 (6), 422–424. https://doi.org/10.1007/BF03047422.
Carey, D.M., Korenowski, G.M., 1998. Measurement of the Raman spectrum of liquid water. J. Chem. Phys. 108 (7), 2669–2675. https://doi.org/10.1063/1.475659.